

Compact Curved Coupler with Novel Flexible Nanocrystalline Flake Ribbon Core for Autonomous Underwater Vehicles

Chen Chen, C. Q. Jiang, *Member*, Yibo Wang, Yuanshuang Fan, Bo Luo, and Yuan Cheng, *Member, IEEE*

Abstract—Conventionally, the magnetic core in an inductive power transfer (IPT) system is spliced by pieces of ferrites, which is time-consuming and unable to realize a seamless fit on the curved surface. This letter proposes a compact curved coupler with a novel flexible nanocrystalline flake ribbon (NFR) magnetic core. Compared with ferrite core, the NFR not only enhances the application flexibility of the IPT system but also significantly reduces its weight in certain power. Based on the LCC-S compensation topology, a 1 kW IPT prototype for autonomous underwater vehicles (AUVs) is fabricated. The transmission characteristics and temperature performance of the system have been investigated under three power levels, considering various permeability values for NFR cores. Finally, the NFR with a permeability of 800 is chosen as the magnetic core, and the DC-DC system efficiency reaches 92.85%. Moreover, it is possible to restrict the maximum temperature to 54.1 °C, and the weight of the NFR cores accounts for merely 4.65% of the whole coupler.

Index Terms—Autonomous underwater vehicles, inductive power transfer, curved coupler, nanocrystalline flake ribbon, configurable permeability.

I. INTRODUCTION

As essential equipment, autonomous underwater vehicles (AUVs) play a vital role in ocean detection, pipeline maintenance, and military patrol [1]-[2]. However, the cruise time is always limited because of the low energy capacity. Inductive power transfer (IPT) technology is regarded as a safe and effective energy supply method for AUVs in the future [3].

Except for high transmission efficiency, lightweight design and system reliability are the main concerns for AUV IPT

This work was supported in part by the Natural Science Foundation of China, China, under Grant 52107011, in part by the Innovation and Technology Commission, Hong Kong SAR, under Grant ITS/068/21, in part by the Research Grants Council, Hong Kong SAR under ECS Grant 21200622, in part by the Science Technology and Innovation Committee of Shenzhen Municipality, China, under Grant SGDX20210823104003034. (*Corresponding author: Chaoqiang Jiang.*)

Chen Chen, C. Q. Jiang, Yibo Wang, Yuanshuang Fan are with the Department of Electrical Engineering and the State Key Laboratory of Terahertz and Millimeter Waves, City University of Hong Kong, Hong Kong, and also with the City University of Hong Kong Shenzhen Research Institute, Shenzhen 518057, China (e-mail: CHEN.Chen@my.cityu.edu.hk; chjiang@cityu.edu.hk; yibwang2-c@my.cityu.edu.hk; yuanshan@my.cityu.edu.hk).

Bo Luo is with the Yantai Research Institute, Harbin Engineering University, China (email: boluo@hrbeu.edu.cn).

Cheng Yuan is with the Department of Electrical Engineering and Automation, Harbin Institute of Technology, Harbin 150001, China, and also with the Chongqing Research Institute, Harbin Institute of Technology, Chongqing 401135, China (e-mail: chengyuan@hit.edu.cn).

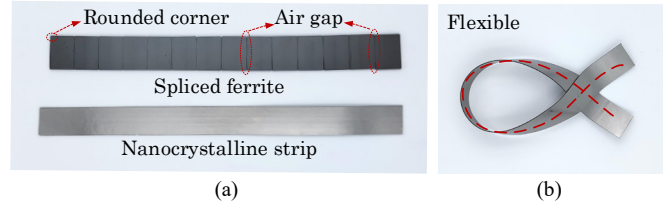


Fig. 1. Magnetic core for the curved coupler. (a) Spliced ferrites and single nanocrystalline strip. (b) Proposed compact flexible flake nanocrystalline.

systems. Compact couplers of a lightweight and suitably shaped coil are good for reducing water impedance. A fit-to-surface and lightweight magnetic coupler was designed in [4], which is composed of an arc bipolar transmitter and a compact dipole-coil-based receiver. It is vertically placed in the middle of the transmitter, allowing more magnetic flux to flow through the receiver. But, the bulky ferrites in both the primary and secondary sides are too heavy. Based on the design idea of [4], an overlapped direct-quadrature (DQ) transmitter is replaced for the bipolar transmitter [5]. Although the double-winding layers ensure consistent magnetic strength across a wide range, a large volume of coil and ferrite is still needed. A novel free-rotation coupler incorporating six receiver coils connected in series and wound in adjacent reverse is proposed for the AUV IPT system, and the output power reaches 700 W [6].

In the abovementioned works, ferrite magnetic cores are utilized to increase the coupling coefficient and improve the transmission efficiency. Typically, a piece of ferrite is made into small boxes with rounded corners, resulting from the angular shape in the manufacturing mold, as shown in Fig. 1(a). The presence of unavoidable air gaps caused by the rounded corners will lead to flux leakages, ultimately leading to a degradation in coupling degree. Besides, when constructing the desired magnetic core, ferrite needs to be spliced together, which cannot fit well on a curved surface. In contrast, the nanocrystalline strip is consecutive and flexible, as shown in Fig. 1(b), eliminating the need for time-consuming splicing processes. This characteristic makes it highly suitable for compact curved couplers.

Flexible nanocrystalline cores with only 0.3 mm thickness are attached to the arc-shaped coupler to decrease the coupler size [7]. Due to the metal-based material, however, nanocrystalline cores will bring more eddy current loss and degrade the transmission efficiency in a high-frequency magnetic field. To address this issue, a laminated nanocrystalline core has been introduced to reduce the eddy current losses [8]. Additionally, a nanocrystalline flake ribbon

> REPLACE THIS LINE WITH YOUR MANUSCRIPT ID NUMBER (DOUBLE-CLICK HERE TO EDIT) <

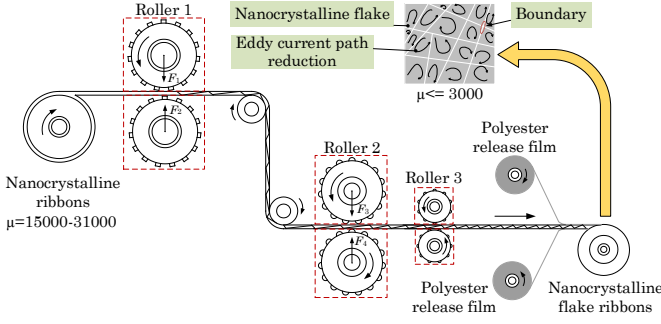


Fig. 2. Crushing process of NFR with configurable permeability.

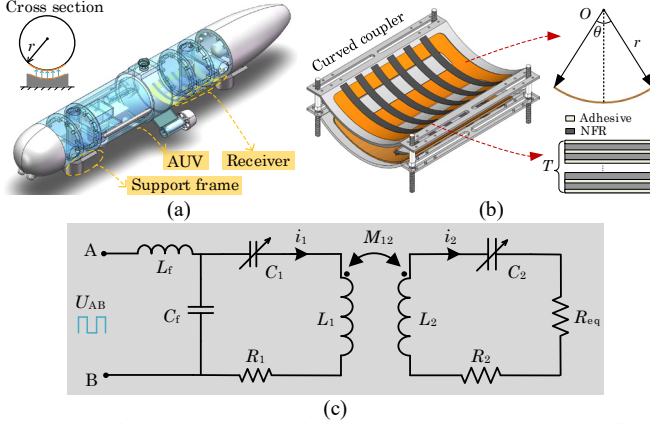


Fig. 3. Curved coupler on AUV and its configuration. (a) Receiver installed on the arc surface of the AUV. (b) Configuration of the curved coupler and multi-layer NFR core. (c) LCC-S compensation topology.

(NFR) core has been proposed, aiming to minimize the eddy current losses [9]. The process of manufacturing the NFR involves bonding them together using laminated adhesive and crushing the nanocrystalline ribbon into fine flakes. Although the flaking process on NFR will reduce its permeability, the high initial permeability ensures the final NFR has a relatively high permeability and acceptable coupling coefficient of the coupler [10]. High saturation ability makes it possible to be used in high-power IPT systems or designed with very thin thicknesses at the same power level compared with ferrite [11]. Moreover, the high flexibility and configurable permeability of NFR provide chances for it to serve as a substitute for conventional ferrite in IPT systems.

This letter proposes a very compact curved coupler with novel NFR cores for the AUV IPT system, which has been rarely studied before. It has much improvement in magnetic core weight, lowering to 4.65% of the whole coupler. Transmission characteristics and temperature performance in six magnetic core groups are investigated in the experiment under three power levels. A double-side NFR core with 800 permeability is chosen for the final AUV IPT system. At a power level of 1 kW, it is possible to achieve a DC-DC system efficiency of 92.85%. The primary objective of this letter is to explore the properties of the flexible NFR magnetic core in curved IPT systems, offering a fresh design reference for the development of lightweight and curved couplers.

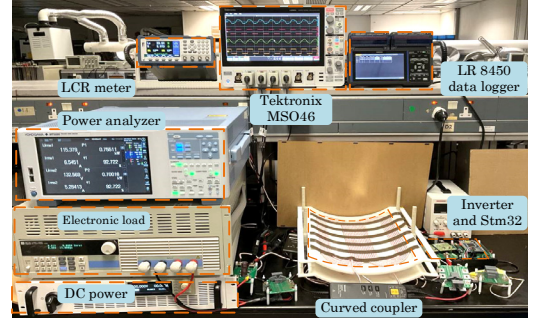


Fig. 4. Experimental platform for curved IPT system.

TABLE I PARAMETERS OF THE CURVED IPT SYSTEM

	NFR1 $\mu=800$	NFR2 $\mu=1500$	NFR3 $\mu=2000$	NFR4 $\mu=3000$	NFR5 No flake	NiZn film
$L_1/\mu\text{H}$	73.13	73.38	76.70	77.75	83.86	53.76
$L_2/\mu\text{H}$	69.1	73.36	73.97	74.32	76.14	70.19
C_1/nF	70.12	64.95	64.59	64.02	62.55	69.31
C_2/nF	47.64	47.61	45.71	45.03	41.82	65.31
k	0.370	0.379	0.389	0.395	0.41	0.329

II. CRUSHING PROCESS FOR NFR AND CONFIGURATION OF CURVED COUPLER

The initial permeability of a conventional nanocrystalline ribbon is around 15000-30000, with a higher saturation ability of 1.25 T, while that of ferrite is only 0.45 T. However, the eddy current in the nanocrystalline ribbon is much higher due to lower resistivity. The crushing process shown in Fig. 2 can squash the nanocrystalline into smaller pieces, narrowing the current path and reducing the eddy current loss. The post-annealing ribbons are extremely brittle, therefore, a very thin layer of pressure-sensitive adhesive (PSA/3 μm) will be attached to the surface of the ribbon to keep its integrity. Meanwhile, configurable permeability can be achieved by adjusting the sizes and types of the roller and the stress F_n when crushing. In addition, the inductance detection of a planar coil after the crushing process is used to assure the precise permeability of NFR.

As a flexible and soft material, NFR is suitable for curved installment situations, such as the outside surface of AUV, as shown in Fig. 3(a). Multi-layer NFR with customized thickness can be achieved by sticking single ribbons (15-20 μm) together to increase the coupling between the receiver and transmitter. The cross-section of the stacked NFR core is illustrated in Fig. 3(b), which consists of 17 layers of single NFR, adjacent two NFRs are connected with PSA adhesive (3-5 μm). The symbol T represents the thickness of the stacked NFR core. The r represents the radius of AUV, and θ is the bending angle of the coupler. In this letter, take $r = 0.2$ m and $\theta = 72^\circ$ as an example for further analysis. LCC-S compensation topology is used in this letter and its equivalent circuit is shown in Fig. 3(c). The values of compensation capacitors C_1 and C_2 are adjustable according to the inductance of L_1 and L_2 .

> REPLACE THIS LINE WITH YOUR MANUSCRIPT ID NUMBER (DOUBLE-CLICK HERE TO EDIT) <

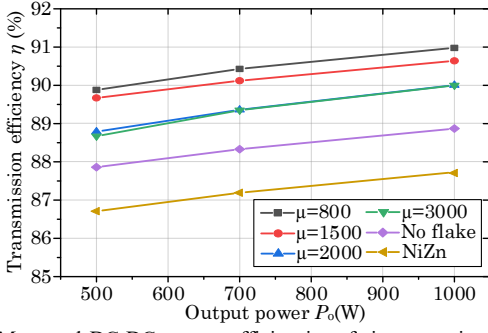


Fig. 5. Measured DC-DC system efficiencies of six magnetic core cases under three power levels of 500 W, 700 W, 1 kW.

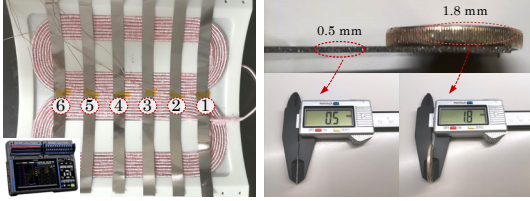


Fig. 7. Arrangement of temperature sensing points and thickness comparison.

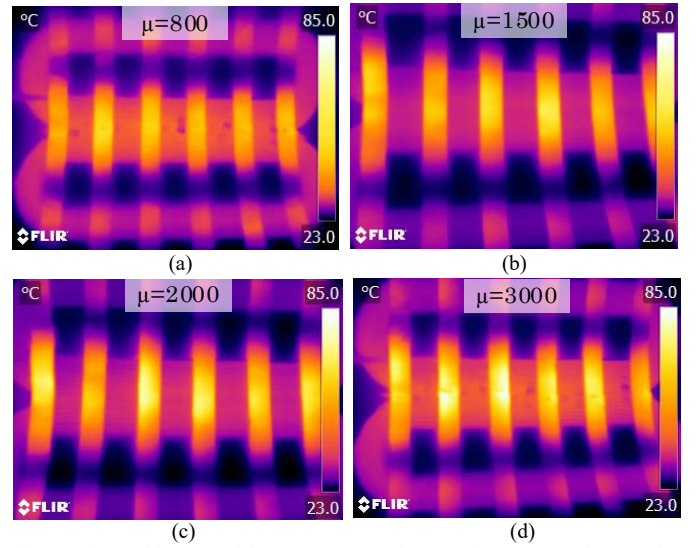


Fig. 6. Thermal images of four NFR cores after 15 minutes operation at 1 kW output power. (a) Permeability with 800. (b) Permeability with 1500. (c) Permeability with 2000. (d) Permeability with 3000.

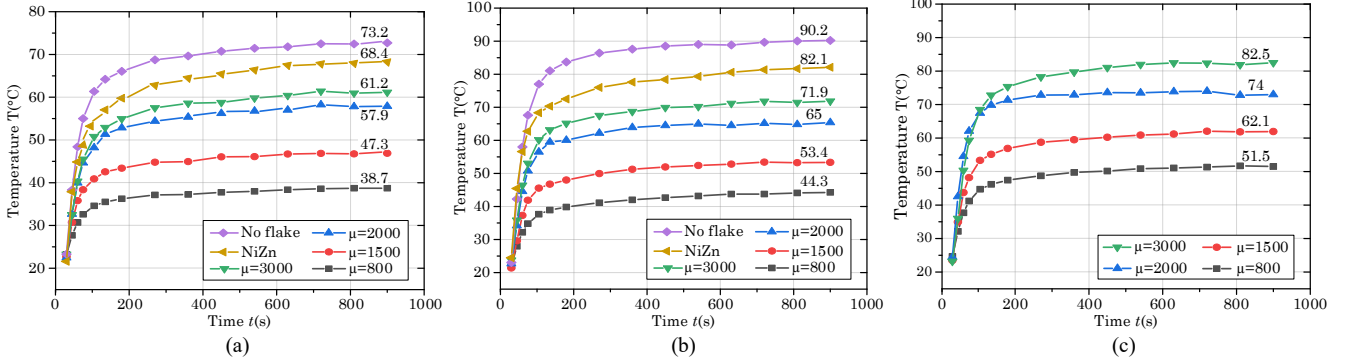


Fig. 8. Measured highest temperatures among 6 sensing points with different nanocrystalline ribbons and NiZn film under different output powers. (a) Output power at 500 W. (b) Output power at 700 W. (c) Output power at 1 kW.

III. EXPERIMENT ANALYSIS FOR AUV IPT SYSTEM

This letter investigates the transmission characteristics and temperature performance of curved IPT systems using five types of NFR cores with permeability of 800, 1500, 2000, 2500, and 3000. B Plus New Materials Technology Co., Ltd provides these nanocrystalline ribbon cores, which have a width of 20 mm and a length of 30 mm. The core thickness is only 0.5 mm with 17 single layers, and the stacking factor is about 0.68. To maintain consistency during the experiments, the permeability of the NFR core on the transmitter remains constant at 2500, while that on the receiver has varying permeability across different groups. It should be noted that the compensation capacitors (C_1 , C_2) need to be recalculated and recompensated to keep the same operation state in each group. The transmission distance is 45 mm, and the working frequency is 85 kHz. The experimental platform is shown in Fig. 4, and the experimental parameters are tableted in Table I. As can be seen from Table I, the coupling coefficient has an increment tendency with the increase of permeability in the groups of nanocrystalline ribbons. The coupling coefficient in NiZn group exhibits the lowest value due to the lowest permeability of NiZn film (permeability is around 150).

According to Kirchhoff's voltage law, the LCC-S compensation topology can be expressed as

$$\begin{bmatrix} U_{AB} \\ 0 \end{bmatrix} = \begin{bmatrix} j\omega L_f + (j\omega C_f)^{-1} \parallel jX_1 - j\omega M_{12} & 0 \\ -j\omega M_{12} & jX_2 + R_{eq} \end{bmatrix} \begin{bmatrix} I_1 \\ I_2 \end{bmatrix} \quad (1)$$

The $R_{eq} = (8 R_L)/\pi^2$ represents the equivalent load of the full-bridge rectifier and electronic load, and $X_1 = \omega L_1 - 1/(\omega C_1)$, $X_2 = \omega L_2 - 1/(\omega C_2)$.

When neglecting the parasitic resistances of coils and the loss of the full bridge inverter and rectifier, the current flowing through the receiver coil and the output power can be calculated as

$$\dot{I}_p = \dot{U}_{AB} / (j\omega L_f), \quad P_o = M_{12}^2 U_{AB}^2 / (R_{eq} L_f) \quad (2)$$

The DC-DC system efficiency can be obtained as follows.

$$\eta = M_{12}^2 \omega / (R_{eq} L_f) \quad (3)$$

A. Transmission characteristic analysis

Fig. 5 demonstrates the DC-DC system efficiency of six groups under three power levels. It can be seen that the system efficiency has a slow climbing tendency as the output power increases. Among the six cases, the NiZn film possesses the lowest system efficiency of 87.73% under 1kW output power, which is the result of the lowest coupling coefficient. Besides,

> REPLACE THIS LINE WITH YOUR MANUSCRIPT ID NUMBER (DOUBLE-CLICK HERE TO EDIT) <

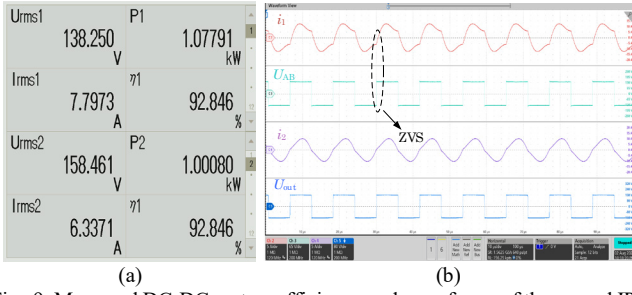


Fig. 9. Measured DC-DC system efficiency and waveforms of the curved IPT system when the output power is 1 kW. (a) DC-DC system efficiency. (b) Waveforms of input, output currents, and voltages.

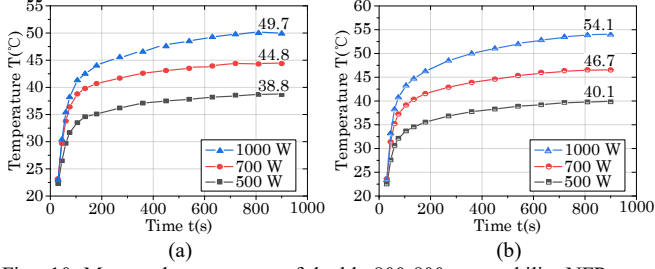


Fig. 10. Measured temperature of double 800-800 permeability NFR cores under different output power. (a) Receiver side. (b) Transmitter side.

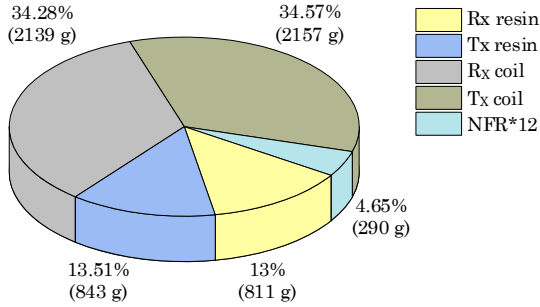


Fig. 11. Weight distribution of curved coupler with NFR cores.

the case of NFR with a permeability of 800 achieves the highest system efficiency. The variation in system efficiency among five nanocrystalline ribbon cores demonstrates that the crushing process can mitigate eddy current losses, even if there is a decrease in permeability.

B. Temperature performance evaluation

The FLIR E6-XT is used to capture the thermal distribution of NFR cores, and six K-type thermocouples connected with the data logger LR8450-HOKIO are used for temperature data recording. The record time is up to 15 minutes, providing sufficient time for system stabilization.

As illustrated in Fig. 6, the heat primarily accumulates in the central concave region of the NFR cores. This phenomenon can be explained by the higher magnetic density in the central part of the double-D (DD) coil. Therefore, the test points (1, 2, 3, 4, 5, 6) for the thermocouple are located at the center of the NFR cores, as shown in Fig. 7. The thickness of the NFR core is only 0.5 mm, which is about 1/3 of the thickness of a coin.

The logged temperature data in three power levels are plotted in Fig. 8. The stable temperature rises with the increment of permeability, proving that the crushing process on NFR cores reduces the eddy current losses. In addition, NiZn film has poorer temperature performance than the NFR cores, whose

permeability is lower than 3000. At the 700 W power level, the maximum temperature recorded for the no-flake nanocrystalline ribbon and NiZn film is 90.2 °C, and 82.1 °C, respectively. Consequently, neither of these materials is utilized at the 1 kW power level to avoid material overheating and burnout. As depicted in Fig. 8(c), the temperature variation in the four NFR groups follows the same trend observed in the 500 W and 700 W power levels.

C. Analysis of NFR core with permeability of 800

Based on the comprehensive analysis of transmission characteristics and temperature distribution across six groups, it can be concluded that the NFR core with a permeability of 800 exhibits a satisfying overall performance. Consequently, the NFR with $\mu=800$ has been implemented as magnetic cores on the surface of the transmitter and receiver in the AUV IPT system for further experiment.

Fig. 9 displays the screenshot of system efficiency captured from the power analyzer WT5000 and the waveforms captured from the oscilloscope under 1 kW output power. P_1 represents the input power, and P_2 represents the output power. The current on the primary side is $I_{1rms}=7.79$ A, and the current on the secondary side is $I_{2rms}=6.33$ A, resulting in a high DC-DC system efficiency of 92.85%. In Fig. 9(b), the primary current i_1 lags off input voltage U_{AB} , demonstrating that the ZVS for a full-bridge inverter can be achieved.

The temperature distribution of NFR cores on the receiver and transmitter side under 1 kW output power is shown in Fig. 10. Compared with Fig. 10(a) and (b), it can be found that the temperature of NFR cores on the transmitter side is higher than that of the receiver side. This disparity can be attributed to the higher current on the primary side, which generates a stronger magnetic density in the surrounding space, resulting in higher eddy current loss on the transmitter side NFR core. Additionally, the temperature shown in Fig. 10 (a) is nearly identical to that of the NFR core with a permeability of 800 in Fig. 8, suggesting that altering the NFR core on the transmitter side does not affect the temperature distribution on the receiver side.

In addition, the weight distribution of the curved coupler is presented in Fig. 11. The total weight of the coupler amounts to 6240 g, with approximately 26.51% attributed to the model resin for coil installation. The Litz wire used in the transmitter and receiver sides accounts for 68.85% of the total weight. The weight of the 12 NFR strip cores is merely 290 g, representing only 4.65% of the overall coupler. The results show that a 0.5 mm thick NFR core with a permeability of 800 is sufficient for a 1 kW IPT system, and the NFR cores will not pose much weight concerns for the entire AUV system.

IV. CONCLUSION

This letter proposes a very compact curved coupler with a thin NFR core for the AUV IPT system. It has satisfying features of lightweight, high transmission efficiency, and exceptional temperature reliability. The experimental results of the thermal distribution reveal that the crushed NFR exhibits lower eddy current losses compared to the no-flake NFR core. Furthermore, it is observed that eddy current losses will be decreased with the increasing degree of crushing. The experiment results show that the DC-DC system efficiency is

> REPLACE THIS LINE WITH YOUR MANUSCRIPT ID NUMBER (DOUBLE-CLICK HERE TO EDIT) <

up to 92.85%, and the maximum temperature is only 54.1 °C when operating at 1 kW output power, while that of NiZn goes for 82.1 °C under 700 W operation. Also, the weight of the NFR core counts for merely 4.65% of the curved coupler. These results highlight the potential of the novel NFR core, which possesses configurable permeability, to replace ferrite in future compact IPT systems.

REFERENCES

- [1] F. Yu, B. He, and J.-X. Liu, "Underwater Targets Recognition Based on Multiple AUVs Cooperative via Recurrent Transfer-Adaptive Learning (RTAL)," *IEEE Trans. Veh. Technol.*, vol. 72, no. 2, pp. 1574–1585, Feb. 2023.
- [2] I. Jawhar, N. Mohamed, J. Al-Jaroodi, and S. Zhang, "An Architecture for Using Autonomous Underwater Vehicles in Wireless Sensor Networks for Underwater Pipeline Monitoring," *IEEE Trans. Ind. Inf.*, vol. 15, no. 3, pp. 1329–1340, Mar. 2019.
- [3] C. Yang, M. Lin, and D. Li, "Improving Steady and Starting Characteristics of Wireless Charging for an AUV Docking System," *IEEE J. Oceanic Eng.*, vol. 45, no. 2, pp. 430–441, Apr. 2020.
- [4] C. Cai, S. Wu, Z. Zhang, L. Jiang, and S. Yang, "Development of a Fit-to-Surface and Lightweight Magnetic Coupler for Autonomous Underwater Vehicle Wireless Charging Systems," *IEEE Trans. Power Electron.*, vol. 36, no. 9, pp. 9927–9940, Sep. 2021.
- [5] S. Wu, C. Cai, A. Wang, Z. Qin, and S. Yang, "Design and Implementation of a Uniform Power and Stable Efficiency Wireless Charging System for Autonomous Underwater Vehicles," *IEEE Trans. Ind. Electron.*, vol. 70, no. 6, pp. 5674–5684, Jun. 2023.
- [6] Z. Yan et al., "Free-Rotation Wireless Power Transfer System Based on Composite Anti-Misalignment Method for AUVs," *IEEE Trans. Power Electron.*, vol. 38, no. 4, pp. 4262–4266, Apr. 2023.
- [7] D. Wang, S. Cui, J. Zhang, Z. Bie, K. Song, and C. Zhu, "A Novel Arc-Shaped Lightweight Magnetic Coupler for AUV Wireless Power Transfer," *IEEE Trans. on Ind. Applicat.*, vol. 58, no. 1, pp. 1315–1329, Jan. 2022.
- [8] D. E. Gaona, S. Ghosh, and T. Long, "Feasibility Study of Nanocrystalline-Ribbon Cores for Polarized Inductive Power Transfer Pads," *IEEE Trans. Power Electron.*, vol. 35, no. 7, pp. 6799–6809, Jul. 2020.
- [9] X. Li, C. Jiang, H. Zhao, B. Wen, Y. Jiang, and T. Long, "Novel Flexible Nanocrystalline Flake Ribbons for High-Frequency Transformer Design," in *2021 IEEE Applied Power Electronics Conference and Exposition (APEC)*, Phoenix, AZ, USA: IEEE, Jun. 2021, pp. 2891–2896.
- [10] C. Jiang, X. Li, S. S. Ghosh, H. Zhao, Y. Shen, and T. Long, "Nanocrystalline Powder Cores for High-Power High-Frequency Applications," *IEEE Trans. Power Electron.*, pp. 1–1, 2020.
- [11] D. E. Gaona, C. Jiang, and T. Long, "Highly Efficient 11.1-kW Wireless Power Transfer Utilizing Nanocrystalline Ribbon Cores," *IEEE Trans. Power Electron.*, vol. 36, no. 9, pp. 9955–9969, Sep. 2021.
- [12] Z. Luo, X. Li, C. Jiang, and T. Long, "Characterization of Nanocrystalline Flake Ribbon for High Frequency Magnetic Cores," *IEEE Trans. Power Electron.*, vol. 37, no. 12, pp. 14011–14016, Dec. 2022.